Biomass Conversion and Biorefinery (2024) 14:17927–17940
https://doi.org/10.1007/s13399-023-03781-1

ORIGINAL ARTICLE

Bioremoval of rhodamine B dye from aqueous solution by using agricultural solid waste (almond shell): experimental and DFT modeling studies

Zeynep Mine Şenol[1] · Noureddine El Messaoudi[2] · Yasmine Fernine[3] · Zehra Seba Keskin[4]

Received: 25 November 2022 / Revised: 7 January 2023 / Accepted: 9 January 2023 / Published online: 17 January 2023

Abstract

The current study aimed to investigate the biosorption of rhodamine B from aqueous solution using an almond shell as an agricultural solid waste biosorbent. The almond shell biosorbent was characterized via Fourier transform infrared spectroscopy (FT-IR), scanning electron microscope (SEM) with energy dispersive X-ray (EDX), and point of zero charge (pH_{PZC}) analyses. The parameters that influence the biosorption process such as contact time, initial dye concentration, biosorbent dose, temperature, and pH were investigated. According to the correlation coefficient, the data were best outlined by the Langmuir isotherm with adsorption capacity of 14.70 mg g^{-1}. The adsorption energy found from the D-R model showed that the adsorption process is chemical. The kinetic data were described by the pseudo-second-order kinetic and intraparticle diffusion kinetic models. Thermodynamic parameters were calculated; it was seen that the biosorption process is spontaneous and endothermic. The density functional theory (DFT) calculation results are well-matched with those discovered through experimentation. The results indicate that almond shells could be interesting alternative material used for dye removal from aqueous solutions.

Keywords Biosorption · Almond shell · Rhodamine B · Kinetic · Isotherms · DFT calculation

1 Introduction

Water pollution has increased substantially in recent decades due to population growth and rapid developments in infrastructure, industrial, agricultural, and pharmaceutical sectors. The main contaminants typically found in water bodies include dyes, pharmaceutical waste, heavy metals, radioactive materials, fertilizers, and pesticides [1, 2]. Dyes consist of synthetic aromatic compounds along with different functional groups [3, 4]. The discharge of wastewater with such dyes into the environment causes many problems which have a detrimental effect on human health and aquatic life [5]. These dyes are synthetic and composed of complex aromatic structures that may be carcinogenic and non-biodegradable [6]. Among them, Rd-B is one of the dyes found in industrial wastewater. Rhodamine B is a highly water-soluble dyestuff with the chemical formula $C_{28}H_{31}ClN_2O_3$ (479.02 g mol^{-1}). Rd-B is a dye with amphoteric properties, although it is generally included in the dyestuff group with basic properties. Therefore, the chromophore groups that give color to the dyestuffs form the cation group of the molecule. The oxochromes, which provide the binding affinities of dyestuffs, are dimethylamino groups in the molecular structure, and chromophore groups are connected by quinoid rings [7, 8]. Rd-B dye is used in the textile industry for coloring papers, dying cotton, wood, leather, and silk [9]. Rd-B causes produce harmful effects such as tissue necrosis in humans, heartbeat increase, shock, and vomiting. Therefore, it is important to develop low-cost approaches that balance cost and effectiveness to remove organic contaminants from residual waters to enable its proper handling either for safe waste disposal or for safe reutilization for human use. Various physical or chemical methods such as ion exchange, reverse osmosis, chemical precipitation, membrane filtration,

✉ Zeynep Mine Şenol
msenol@cumhuriyet.edu.tr

[1] Department of Nutrition and Diet, Faculty of Health Sciences, Cumhuriyet University, Sivas 58140, Turkey

[2] Laboratory of Applied Chemistry and Environment, Faculty of Sciences, Ibn Zohr University, 80000 Agadir, Morocco

[3] Engineering Laboratory of Organometallic, Molecular Materials and Environment, Sidi Mohamed Ben Abdellah University, 30000 Fez, Morocco

[4] Department of Pharmacy, Health Services Vocational School, Cumhuriyet University, Sivas 58140, Turkey

and adsorption are used for the treatment of wastewater [10]. In the removal of colored pollutants from wastewater, the adsorption process has the advantages of low cost, high selectivity, efficiency, environmental friendliness, and ease of application [11–13]. For the adsorption process to be applied more effectively, it is of particular importance that the material chosen as an adsorbent is economical, easily obtainable, easily recoverable, and non-toxic [4, 14–16]. For this purpose, the use of cheap, non-toxic, abundant in nature, low-cost adsorbents has become widespread in recent years. Natural minerals and polymers are widely used such as clay [17], vermiculite [18], sepiolite [19], and dolomite [20] and natural minerals such as chitosan [21] and lignin [22] in the removal of dyes from wastewater. In addition to these adsorbents, the use of biosorbent, which is defined as the removal of dyes by living or dead biomass, stands out today. The biosorption process is very attractive because the biosorbent is inexpensive and readily available. Today, various agricultural solid wastes as natural biosorbent such as agave bagasse [23], apricot stone [24], grapefruit peel [25], corncob [26], avocado seed [27], and bamboo shoot shell [28] were utilized for the removal of dyes from wastewater. The use of agricultural solid waste biomass as a biosorbent is very interesting due to its advantages such as the high potential for ion exchange, the biosorbent recovery by sorption–desorption cycles, the low cost and easy availability, the abundance, and the high surface area [29, 30].

Therefore, this study investigates the feasibility of using an almond shell (AS)-based biosorbent to remove Rd-B as a cationic dye from an aqueous solution. AS is a readily available lignocellulosic biowaste feedstock that contains cellulose, hemicellulose, and pectic components. The experiments were designed, and the operating conditions were optimized. Isotherm and kinetic studies were also carried out to identify the adsorption properties of the biosorbent. To our knowledge, this is the first report on the removal of Rd-B dye using AS biosorbent. Moreover, this study also involves quantum chemical calculations. Quantum chemical parameters were calculated by the DFT/B3LYP/6-311G method for the unprotonated and protonated Rd-B. Finally, to prove the effective application of the material, we treat wastewater from paper photography processing operations using AS biosorbent showing efficient removal of organic contaminants.

2 Methods

2.1 Reagents and instrumentation

2.1.1 *Reagents*

Rd-B and methanol were purchased from Sigma-Aldrich. HCl, NaOH, KNO_3, and ethanol were all purchased from Merck. Other all chemicals were of analytical grade.

2.1.2 Instrumentation

FT-IR (Bruker Model: Tensor II), SEM–EDX (SEM Tescan Mira3 Xmu), and UV–vis spectrophotometer "Shimadzu 160A" measuring device.

2.2 Preparation of biosorbent

The almond shells called *Prunus dulcis* were obtained from the Kaynarlar company in Tokat province in Turkey. After collection samples were washed with distilled water, dried at room temperature, and then used and stored in a polypropylene container for use in biosorption experiments.

2.3 Biosorption experiments

To understand the nature of the biosorption process, experiments were carried out in a 10 mL solution volume polypropylene tube, at 500 mg L^{-1} Rd-B dye concentration, at natural solution pH: 5.8, in 100 mg biosorbent mass, and at 25 °C for 24 h carried out. The solution was then vigorously stirred, and after 24 h, the concentration of Rd-B dye in the equilibrium solution was determined by absorbance measurement at $\lambda = 554$ nm using a UV–vis spectrophotometer [31]. Biosorption%, Q (mg g^{-1}), and recovery% were calculated in Eqs. 1, 2, and 3, respectively.

$$Biosorption\% = \left[\frac{C_i - C_f}{C_i}\right] \times 100 \quad (1)$$

$$Q = \left[\frac{C_i - C_f}{m}\right] \times V \quad (2)$$

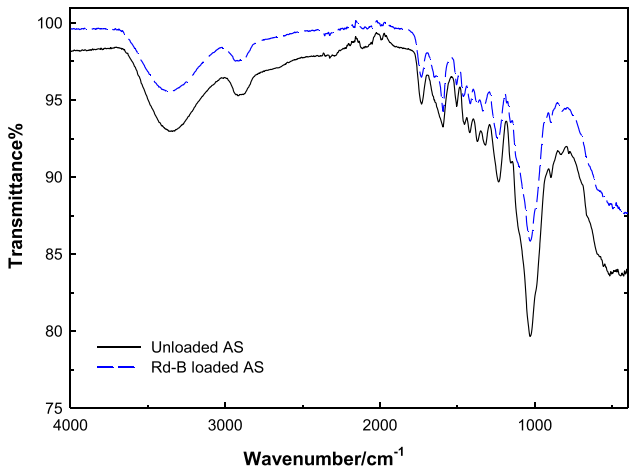

Fig. 1 FT-IR spectra of unloaded (**a**) and Rd-B loaded AS (**b**)

$$\text{Recovery}\% = \frac{Q_{\text{des}}}{Q_{\text{ads}}} x100 \tag{3}$$

C_i, C_f, m, and V represent the initial and equilibrium liquid-phase concentrations of the Rd-B dye (mg L^{-1}), the biosorbent mass (mg), and the volume of the solution (L), respectively [32–34].

2.4 Computation details

Quantum chemical calculations are important to describe the quantum chemical parameters of the molecule, such as molecular orbital energy HOMO and LUMO, gap energy, dipole moment (μ), softness (σ), and total energy (ET). All calculations were made with Gaussian 09 software [35] the geometry of the molecules studied was fully optimized using the DFT/B3LYP/6-311G in the aqueous phase. The quantum parameters are presented by mathematical formulas as follows (Eqs. 4–7):

$$\Delta E_{\text{gap}} = E_{\text{LUMO}} - E_{\text{HOMO}} \tag{4}$$

$$\chi = \frac{-\left(E_{\text{LUMO}} + E_{\text{HOMO}}\right)}{2} \tag{5}$$

$$\eta = \frac{\left(E_{\text{LUMO}} - E_{\text{HOMO}}\right)}{2} \tag{6}$$

$$\sigma = \frac{1}{n} \tag{7}$$

3 Results and discussion

3.1 FT-IR and SEM–EDX analysis

On almond shells FT-IR (Fig. 1), the broad flattened peak was observed at 3281 cm^{-1} attributed to the OH group. Peak

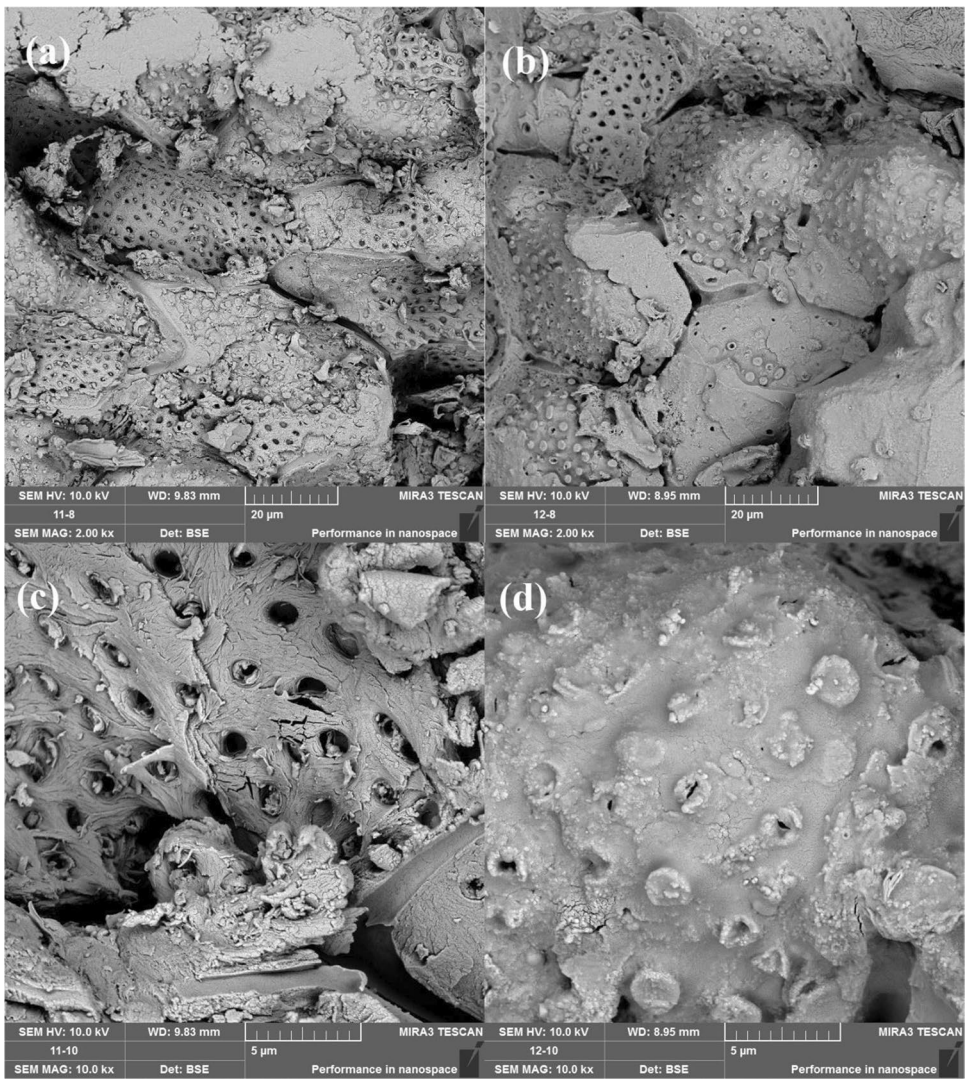

Fig. 2 SEM photographs of AS biosorbent before (**a**, **c**) and after (**b**, **d**) biosorption of Rd-B

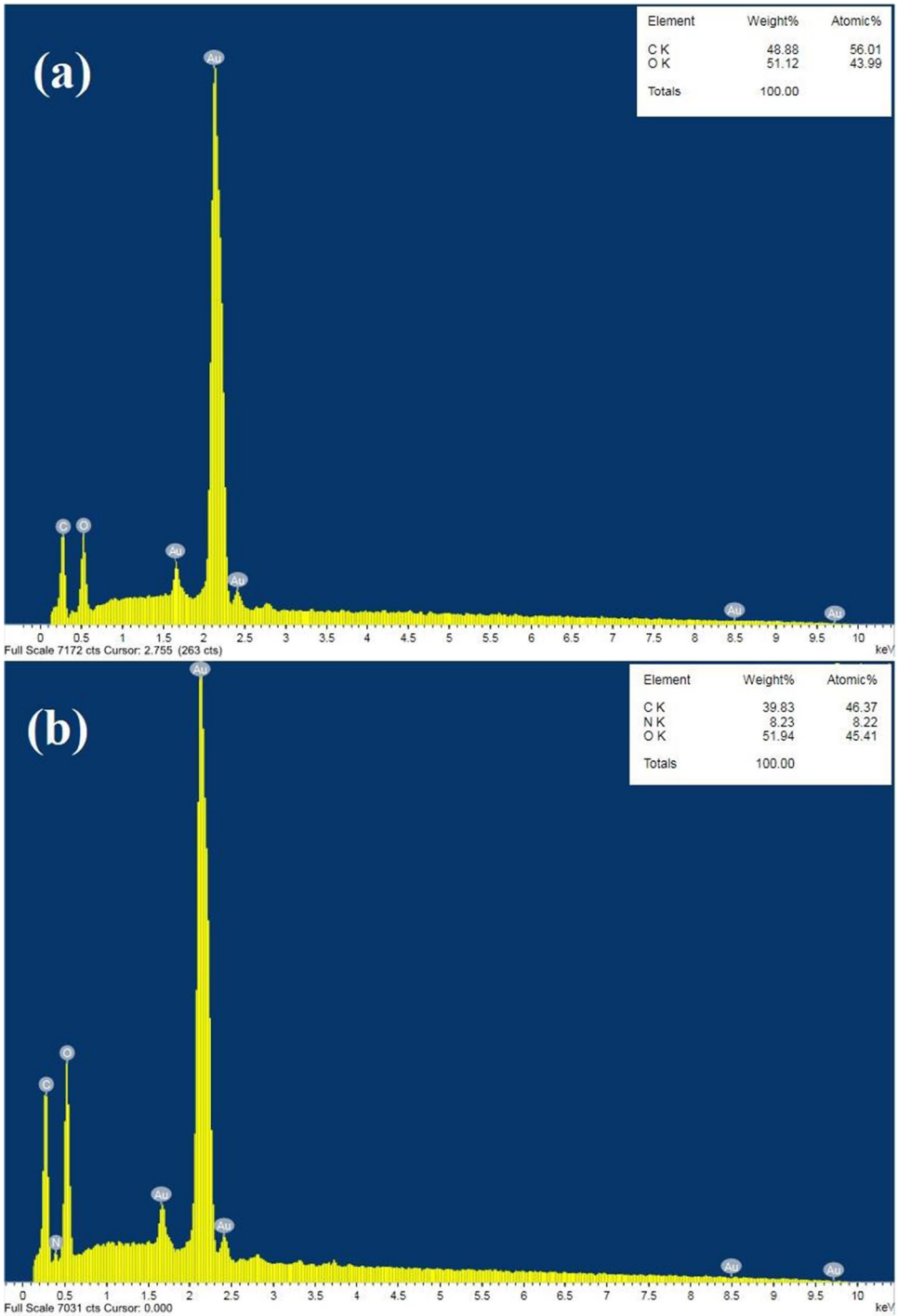

Fig. 3 EDX spectrum of AS biosorbent before (**a**) and after (**b**) biosorption of Rd-B

intensity increased to 2820 cm^{-1} showing the symmetric and asymmetric stretching of the C-H bond of the CH_2 group. The broadbands in the region of 1750–1000 cm^{-1} are characteristic of the stretching of C = O, C-O groups and bending vibrations of adsorbed water [36]. Rd-B shows significant changes after biosorption, and the new peak was observed at 1464 cm^{-1} attributed to C-H bending of alkane [37]. Two different new peaks emerge from 973 to 778 cm^{-1} attributed to C = C bending [38]. The spectral changes and new peaks formation confirm the biosorption of Rd-B dye on the almond shells.

SEM analysis was used to observe the morphological differences of AS biosorbent before and after the biosorption of Rd-B dye. The SEM images in Fig. 2a and c show the structure of AS biosorbent before biosorption, and Fig. 2b and d shows the structure after biosorption. Figure 2a and c show

that the structure of the biosorbent is porous and irregular. In the SEM images in Fig. 2b and d, it is clearly observed that after the biosorption, the pores turn into a smoother and more regular structure as they are filled with Rd-B dye molecules. This significant differentiation in the structure of the biosorbent indicates surface complexation.

Elements before and after biosorption on AS biosorbent were determined using EDX analysis, and EDX spectra are given in Fig. 3. The peaks of C and O were determined in the EDX analysis of AS biosorbent before biosorption. After biosorption, the peaks of C, O, and N were determined in the EDX analysis. The presence of N in the structure of the Rd-B dye was evaluated as evidence for biosorption.

3.2 Effect of pH on biosorption and PZC for AS biosorbent

The protonation mechanism of the Rd-B molecule was studied between pH 0 and 14 by the MarvinSketch software. Figure 4 represents the different forms of this molecule and the percentage of protonation sites. It is observed that the Rd-B molecule has weak basic properties which facilitate their protonation in the acid medium; also the presence of heteroatoms in the molecule studied also suggests their strong tendency to protonation in acid solution. Figure 4 has illustrated the distribution ratio of each species as a function of pH; it is clear that only one major form (Rd-B-H^+) was 94% at pH = 0 [39]

Generally, for a cationic dye, the percent dye removal will decrease at a low pH solution and increase at high pH solution [40]. Figure 5 depicts the effect of pH on the adsorption capacity. The elimination as a function of pH was investigated at a pH 2.0 to 12.0. We can mark that the maximum dye biosorption was noticed at a pH of 2–6 (acid medium), while the minimum biosorption capacity was at pH of 8–12 (basic medium). By increasing pH value, the concentration of H^+ increase, and the tendency of Rd-B dye molecules to occupy active sites increase leading to a decrease in the quantity biosorbed of AS biosorbent [41]. At high pH, the Rd-B dye molecules may get converted to their hydroxides,

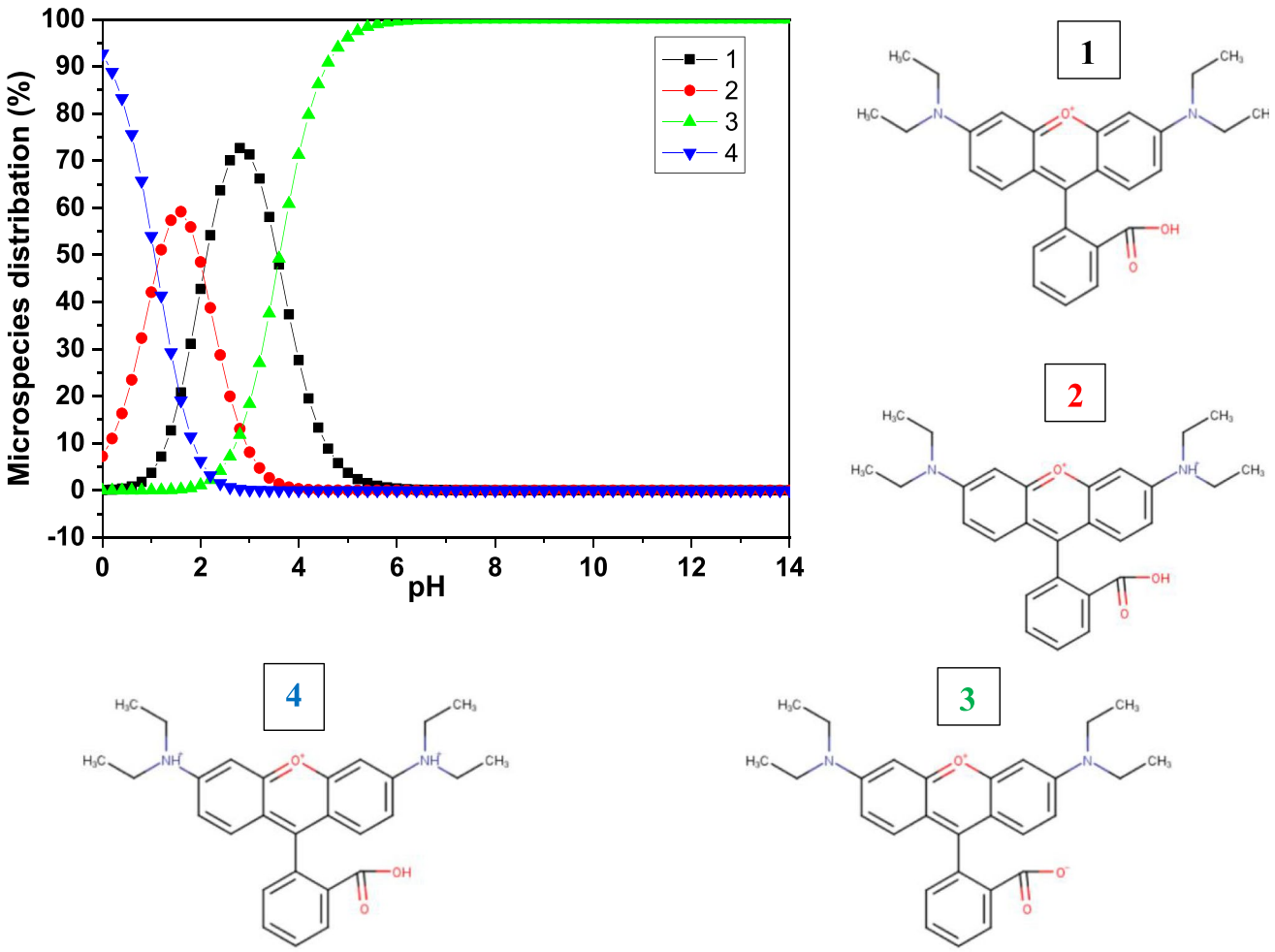

Fig. 4 Speciation diagram for Rd-B as function of pH

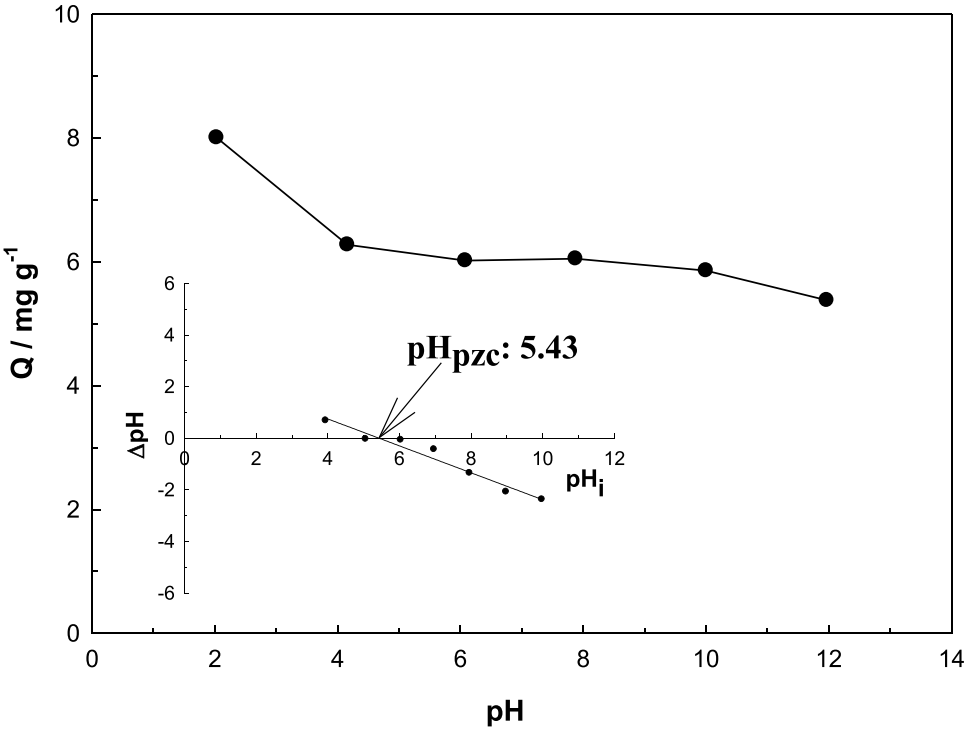

Fig. 5 Effect of pH on biosorption of Rd-B onto AS {[Rd-B]$_0$: 500 mg L^{-1}, biosorbent mass: 10 g L.$^{-1}$, pH: 2.0–12.0, contact time: 24 h, temperature. 25 °C} and pzc for almond shells (*Prunus dulcis*)

resulting in a decrease in the biosorption of Rd-B by the active sites of AS biosorbent [42] The point of zero charge (pzc) of AS biosorbent was 5.43 (Fig. 5). The finding suggests that the biosorbent surface will be positively charged at pH below pH_{pzc}, favoring anionic attraction. On the other hand, the biosorbent becomes negatively charged when the $pH_{pzc} > pH$, favoring cationic attraction [43].

3.3 Effect of biosorbent dose

To study the effect of the biosorbent mass on the retention of Rd-B dye by almond shells powder, we varied the value of the biosorbent dose from 1 to 20 g L^{-1} a concentration of 500 mg L^{-1} of Rd-B dye and a natural pH. All the results are grouped in Fig. 6; it can be seen that the dye removal percentage increases

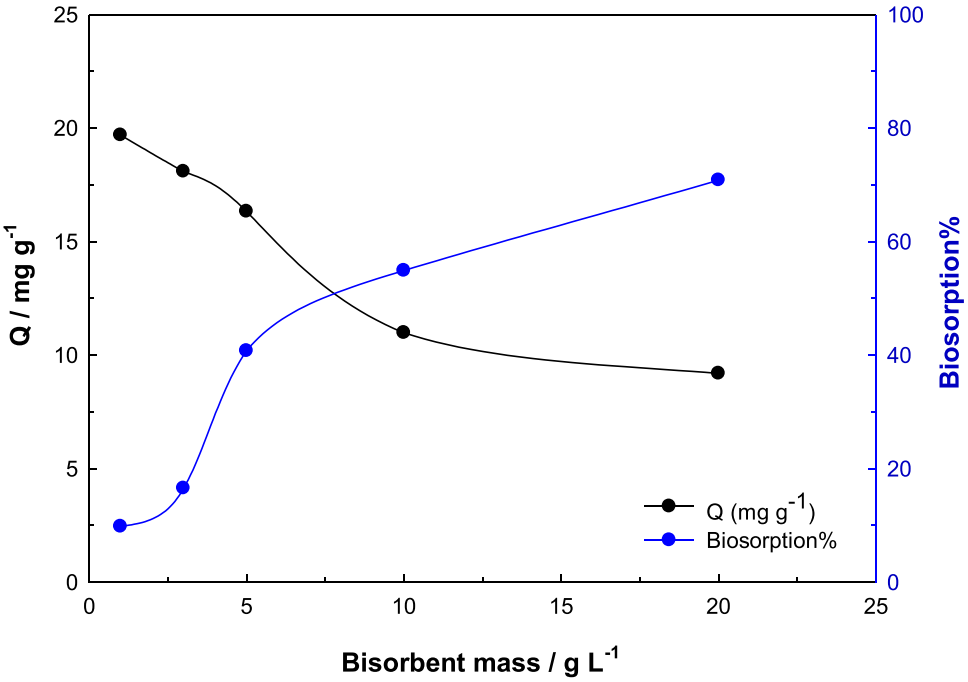

Fig. 6 Effect of biosorbent dose on biosorption of Rd-B dye onto AS {[Rd-B]$_0$: 500 mg L^{-1}, biosorbent mass: 1–20 g L^{-1}, natural pH: 5.8, contact time: 24 h, temperature: 25 °C}

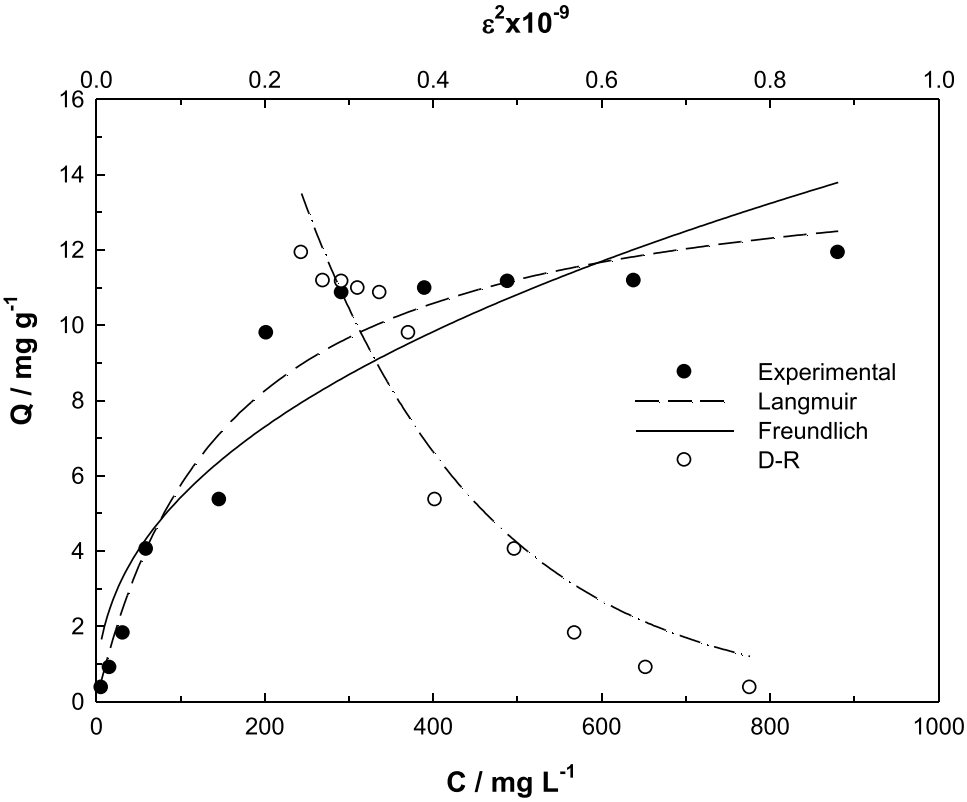

Fig. 7 Biosorption isotherms {[Rd-B]$_0$: 10–1000 mg L^{-1}, biosorbent mass: 10 g L^{-1}, natural pH: 5.8, contact time: 24 h, temperature: 25 °C}

from 9.83 to 70.82% with the biosorbent dose increasing from 1 to 20 g L^{-1} proportionally. This is possibly due to the increase in the number of biosorption sites following the increase in the biosorbent dose [44]. However, the encounter (molecules-site) is more probable, leading to better retention of the Rd-B dye by the AS biosorbent [45]. The biosorbent dose was set at 10 g L^{-1} for the subsequent experiments.

3.4 Biosorption isotherm models

In the current study, Langmuir [46, 47], Freundlich [48], and Dubinin-Radushkevich (D-R) [49] models (Fig. 7) were selected to investigate the interaction between the Rd-B dye molecules and the AS biosorbent surface. The biosorption isotherm model parameters are presented in Table 1; it is seen that the correlation coefficient of the Langmuir model (R^2: 0.960) is larger than the Freundlich model (R^2: 0.886). This showed that Rd-B dye biosorption on AS better fitted the Langmuir model. Rd-B dye biosorption on AS took place in a monolayer. The D-R isotherm model, on the other hand, evaluates biosorption on porous surfaces from an energetic point of view [50]. If the adsorption energy is less than 8 kJ mol^{-1}, it is physical, and if it is between 8 and 16 kJ mol^{-1}, it is chemical. When the Rd-B dye biosorption to the AS biomass is evaluated from this point of view, it is

Table 1 Biosorption isotherms and their parameters

Model	Parameter	Value
Langmuir	X_L (mg g^{-1})	14.7
$Q = \frac{X_L C_e}{1+K_L C_e}$	K_L (L mg^{-1})	0.0064
	R^2	0.960
Freundlich	X_F	0.751
$Q = X_F C_e^{\beta}$	β	0.429
	R^2	0.886
D-R	X_{DR} (mg g^{-1})	40.8
$Q = X_{DR} e^{-(K_{DR}\varepsilon^2)}$	$-K_{DR}\times10^9$/mol^2 KJ^{-2}	4.54
$\varepsilon = RT\ln\left(1+\frac{1}{C_e}\right)$	E_{DR}/kJ mol^{-1}	10.5
$E_{DR} = (2K_{DR})^{-0.5}$	R^2	0.915

Table 2 Comparison of sorbent capacities of low-cost sorbents

Sorbent type	Qm (mg g^{-1})	References
Coffee ground	5.26	[51]
Banana peel	3.88	[52]
Walnut shell	2.29	[53]
Activated carbon	4.93	[54]
Multi-walled carbon nanotubes (MWCNTs)	3.53	[55]
Fe_3O_4/MWCNTs-COOH	11.4	[56]
Starch grafted p-tert-butyl-calix[n]arene	9.81	[57]
Diatomite	8.13	[58]
Almond shells (*Prunus dulcis*)	14.70	This study

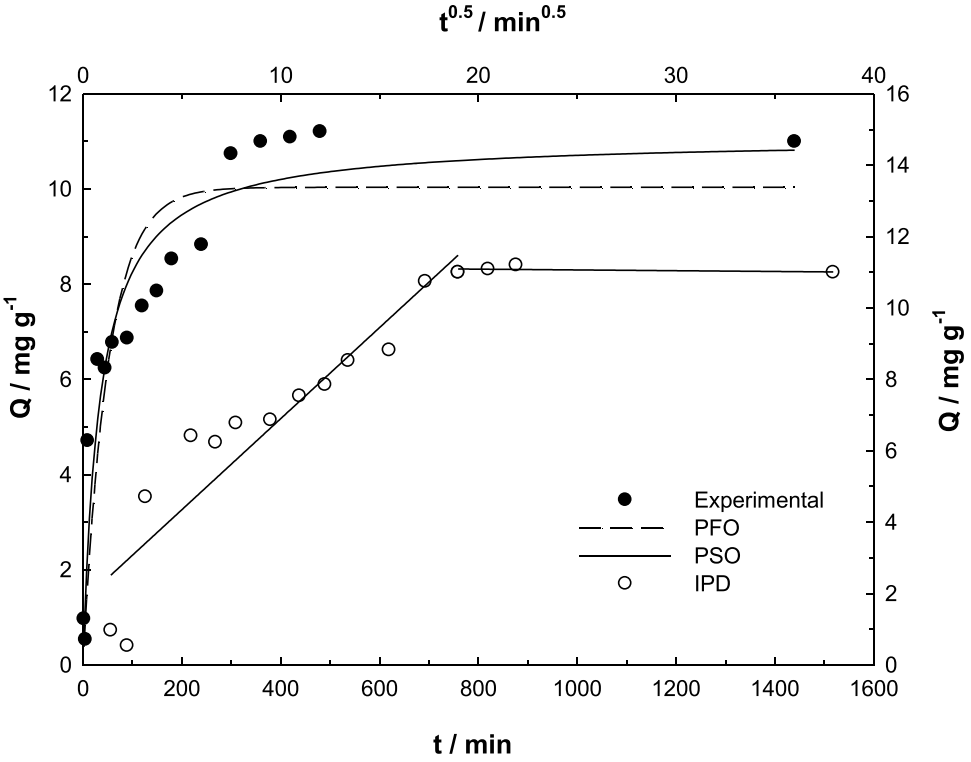

Fig. 8 Biosorption kinetics {[Rd-B]$_0$: 500 mg L^{-1}, biosorbent mass: 300 mg, natural pH: 5.8, contact time: 10–1440 min, temperature: 25 °C}

seen that the E_{DR}: 10.5 kJ mol^{-1} is, in this case, the biosorption process chemical.

Maximum monolayer sorption capacities of Rd-B dye to various sorbents are presented in Table 2. When Table 2 is examined, it is seen that the biosorption capacity of AS biomass is relatively larger compared to other sorbents. This is promising because AS biomass is an effective, inexpensive, and natural biosorbent for the removal of Rd-B dye from wastewater.

3.5 Biosorption kinetics

Biosorption kinetics provide vital information about the rate and mechanism of the biosorption process. Generally, an adsorption process takes place in three stages: (i) mass migration from solution to biosorbent surface, which is very rapid due to mixing, (ii) the film diffusion of the biosorbent from the bulk solution to the surface of the biosorbent, and (iii) the intraparticle diffusion of the biosorbate into the pores of the biosorbent.

Pseudo-first-order (PFO), pseudo-second-order (PSO), and intraparticle diffusion (IPD) models (Fig. 8) [59, 60] are commonly used to explain biosorption kinetics. As a result of the fit to the models, the biosorption mechanism can be predicted. From Table 3, it is seen that the R^2 value of the PSO model (R^2: 0.907) is higher than that of the PFO (R^2: 0.834) model. This showed that Rd-B dye adsorption on AS biomass better fitted the PSO model.

When the IPD model fit graph is examined, it is seen that it has two linear components instead of a single line passing through the origin. In this case, he states that the biosorption process includes firstly rapid adsorption to the surface and then relatively slow intraparticle diffusion steps. This showed that it is not possible to explain the biosorption process with a single kinetic model. The biosorption kinetics of Rd-B dye to AS biomass can be explained by PSO and IPD models [61].

Table 3 The calculated parameters of PFO, PSO, and IPD models

Model	Parameter	Value
PFO	Q_t/mg g^{-1}	11.08
$Q_t = Q_e\left(1 - e^{-k_1 t}\right)$	Q_e/mg g^{-1}	10.04
$H_1 = k_1 Q_t$	$k_1 \times 10^3$/mg^{-1} g min^{-1}	19.4
	$H_1 \times 10^3$/mg g^{-1} min^{-1}	0.195
	R^2	0.834
PSO	Q_t/mg g^{-1}	11.08
$\frac{t}{Q_t} = \frac{1}{k_2 Q_e^2} + \frac{t}{Q_t}$	Q_e/mg g^{-1}	11.07
$H_2 = k_2 Q_t^2$	$k_1 \times 10^3$/mg^{-1} g min^{-1}	2.64
	$H_2 \times 10^3$/mg g^{-1} min^{-1}	323
	R^2	0.907
IPD	$k_i \times 10^3$/mg g^{-1} min$^{-0.5}$	1797
$Q_t = k_i t^{0.5}$	R^2	0.863

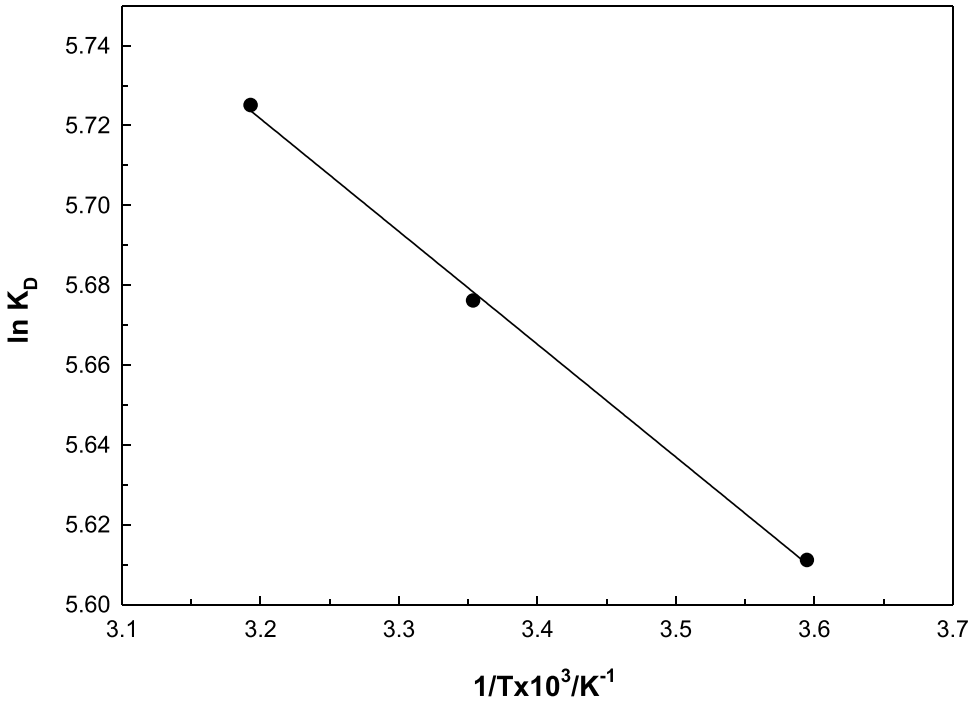

Fig. 9 The effect of temperature {[Rd-B]$_0$: 500 mg L^{-1}, biosorbent dose: 10 g L^{-1}, natural pH: 5.8, contact time: 24 h, temperature: 5 °C, 25 °C, and 40 °C}

3.6 Biosorption thermodynamics

During the biosorption process, thermodynamic parameters such as $\Delta H°$, $\Delta G°$, and $\Delta S°$ were calculated using the following equations [62] $\Delta G°$ was determined using Eq. 8.

$$\Delta G^{\circ} = -RT\ln(K_d) \tag{8}$$

where R (8314 J mol^{-1} K^{-1}) is the ideal gas constant, T (K) is the absolute temperature, and K_d is the distribution coefficient. The dispersion coefficient, which reveals the affinity of the biosorbent surface, is calculated by Eq. 9.

$$K_d = \frac{Q}{C_e} \tag{9}$$

$\Delta H°$ and $\Delta S°$ parameters were found using the Van't Hoff Eq. 10.

$$\ln K_D = \frac{\Delta S^{\circ}}{R} - \frac{\Delta H^{\circ}}{RT} \tag{10}$$

Table 4 Thermodynamic parameters

Temperature/°C	ΔG°/kJ mol^{-1}	ΔH°/kJ mol^{-1}	ΔS°/ Jmol^{-1} K^{-1}	R^2
5	− 12.1	2.35	55	0.999
25	− 14.1			
40	− 15.0			

$\Delta H°$, $\Delta G°$, and $\Delta S°$ were determined using the slope and intercept values of the lnK_D-1/T plot (Fig. 9, Table 4). When Table 4 is analyzed, it is seen that the biosorption process is spontaneous, entropy-increasing, and endothermic.

3.7 Recovery and reusability of AS

The recovery and reusability of AS biosorbent after the biosorption process is extremely important in terms [63, 64]. Therefore, 5 times desorption experiment was carried out using HCl, methanol, and ethanol, solutions with 0.1 mol L^{-1} concentration to recover the Rd-B dye biosorbed on the AS biosorbent surface. Obtained recovery percentages are given in Fig. 10. In Fig. 10, it is seen that the highest recovery is achieved with ethanol (46%), and the lowest recovery is with HCl (23%).

3.8 DFT calculations

3.8.1 Reactivity descriptor analysis

Several quantum chemical parameters have been calculated and summarized in Table 5. The neutral form and the protonated form of the Rd-B molecule can be explained in terms of geometry, and it could be explained in terms of the gap energy ΔE_{gap} and other quantum parameters. Therefore, the lower the energy difference between the orbital HOMO and LUMO, the easier the electrons of the molecule to pass to the surface of the adsorbent, and the higher

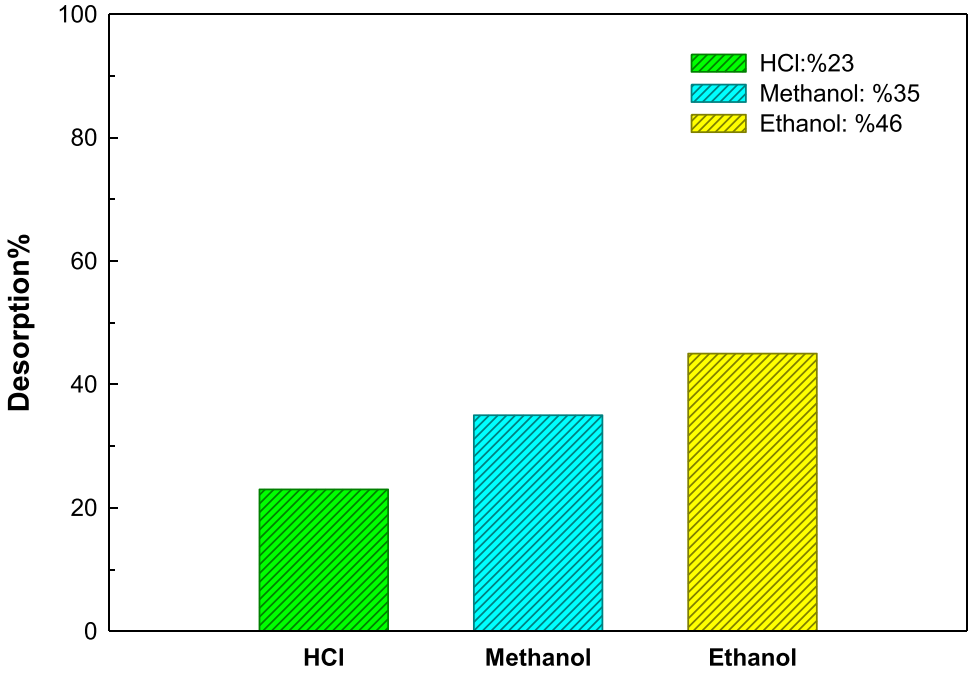

Fig. 10 The effect of desorption on AS biomass

the application of biosorption will be, on the other hand, larger gap values will provide low chemical reactivity [65]. According to the results obtained in Table 5, we note that the proton form (P-Rd-B) has the smallest energy difference (1.3765 eV), so it is the least stable and most reactive form. Chemically relative to the neutral form (Rd-B), the P-Rd-B molecule is the easiest to be adsorbed by the almond shell adsorbent. The proton molecule (P-Rd-B) has a low hardness value ($\eta = 0.6882$ eV) and the highest softness value ($S = 1/\eta = 1.4528$ eV); this suggests the ability to adsorb by the almond shells; also the dipole moment of the protonated form is higher compared to the neutral form; maybe a larger dipole moment is responsible for the biosorption.

Figure 11 represents the frontier orbitals HOMO and LUMO of the neutral and protonated form after optimization. This Fig. 12 confirms that the Rd-B dye molecule is rich in electrons and capable of donating electrons. It is also observed that the HOMO density distribution of Rd-B dye is located on the heterocyclic atom rings, the nitrogen, and the CH_3 groups. The distribution of the HOMO density of protonated form P-Rd-B is located in the function C = C, C–C = C, the oxygen atom, and the nitrogen atom which can play an essential role in the absorption.

3.8.2 The Mulliken charges

Several authors agree that the more the heteroatom is negatively charged, the more it is able to adsorb by the adsorbent and has a serious reaction of the donor–acceptor type. The Mulliken charges for Rd-B and P-Rd-B are reported in Fig. 12. Examination of these results shows that all heteroatoms have negative charges with high electron density. These atoms behave as nucleophilic centers when they interact with the adsorbent. From the values of Fig. 12, it is possible to observe that all the atoms of nitrogen and oxygen have a considerable excess of negative charge, and some carbon atoms have a negative charge, which are adsorbent active atoms.

4 Conclusion

In this study, agricultural solid waste biosorbent (almond shell) was used, and its effectiveness in removing Rd-B dye from aqueous solution was investigated. The maximum biosorption capacity of AS biosorbent for the Rd-B dye was found as 14.7 g mg^{-1} at 25 °C from the Langmuir model.

Table 5 Quantum chemical parameters are calculated by the DFT/B3LYP/6-311G method for the Rd-B and P-Rd-B

Quantum chemical descriptor	E_{HOMO} (eV)	E_{LUMO} (eV)	ΔE_{gap} (eV)	χ (eV)	η (eV)	S (eV)	E_{Tot} (u.a)	Dipole
Rd-B	− 5.8969	− 3.0795	2.8174	4.4882	1.4087	0.7098	− 1421.07	06.26
P-Rd-B	− 7.9848	− 6.6082	1.3765	7.2965	0.6882	1.4528	− 1420.61	10.45

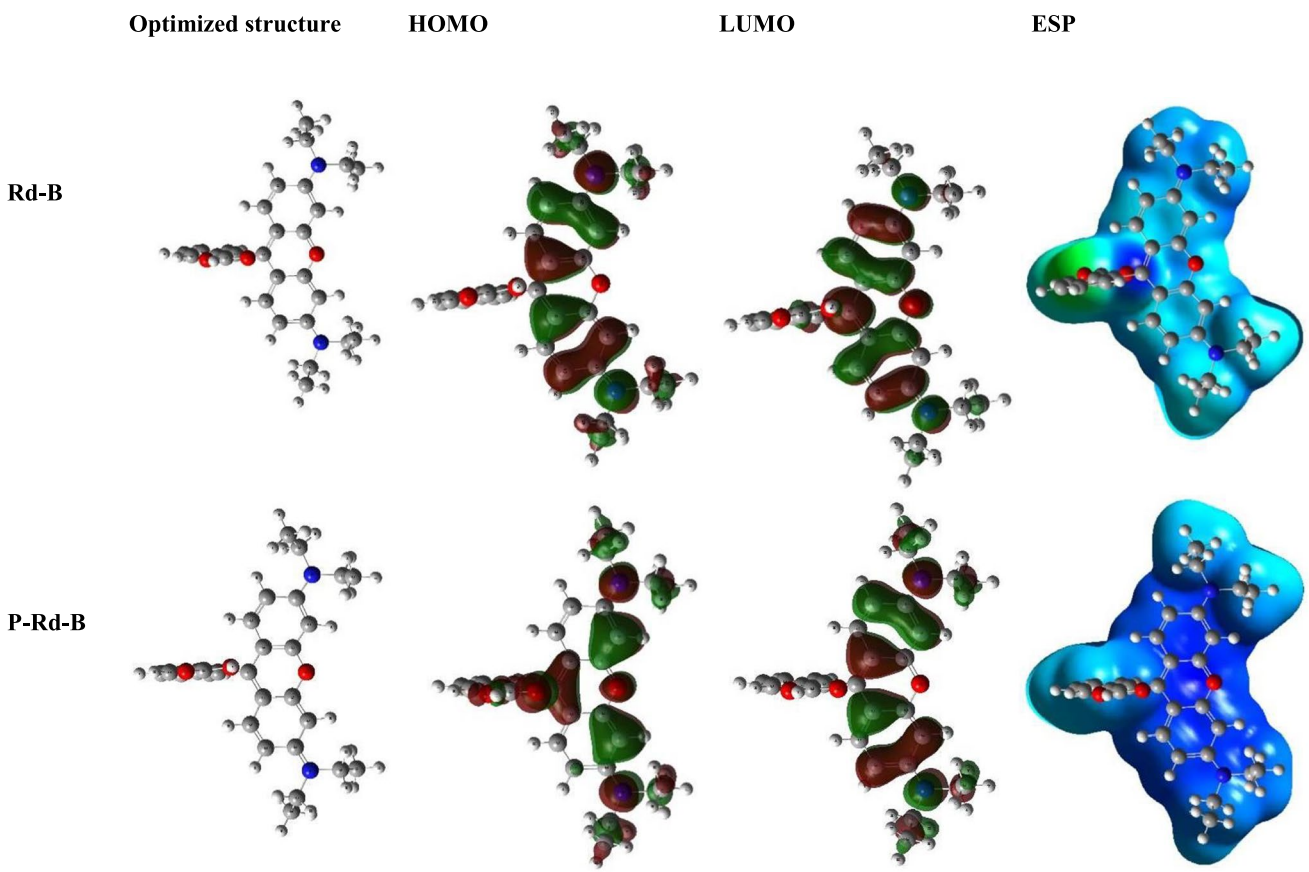

Fig. 11 Representation of the optimized geometry, frontier orbitals (HOMO, LUMO), and electrostatic potential (ESP) of the Rd-B and P-Rd-B

The adsorption energy found from the D-R model showed that the adsorption process is chemical. Adsorption kinetics showed that the adsorption process is quite suitable for PSO and IPD models. Thermodynamic parameters of the biosorption process of Rd-B dye molecules by AS biosorbent were determined. At 25 °C, ΔH^0, 2.35 kJ mol^{-1}; ΔS^0,

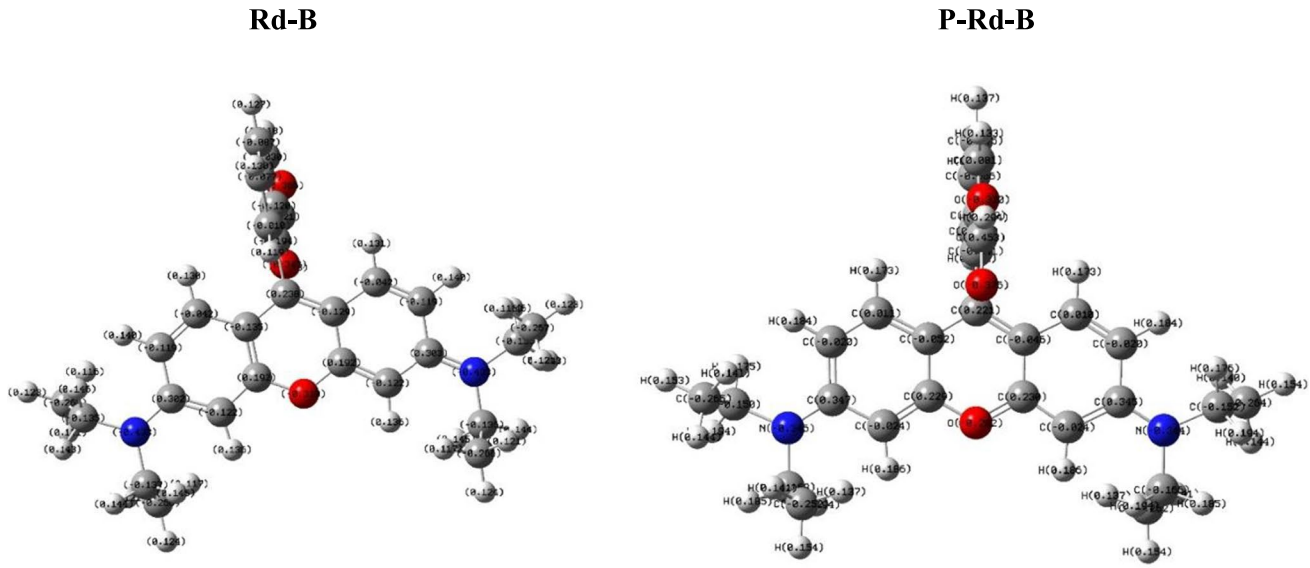

Fig. 12 Mulliken charges for Rd-B and P-Rd-B

55 kJ mol^{-1}; and ΔG^0, − 14.1 kJ mol^{-1} were found. Also, at different temperatures, the adsorption process is negative, so it happens spontaneously. In addition, the adsorption of Rd-B dye molecules on the AS biosorbent surface was demonstrated by FT-IR and SEM–EDX analyses. The adsorption–desorption experiment results showed that the AS biosorbent has very good reusability and stability. The results of this work show that an effective low-cost adsorbent can be produced starting from almond shells without any treatment, which can be used by communities with limited resources facing water contamination by dyes. Moreover, the quantum chemical calculations used allowed us to propose the binding mechanism for Rd-B biosorption to the AS biosorbent. The overall results showed that the AS biosorbent has a remarkable biosorption affinity towards the Rd-B dye in aqueous medium.

Author contribution Zeynep Mine Şenol: conceptualization, data curation, investigation, methodology, project administration, resources, supervision, writing—original draft, writing—review and editing. Noureddine El Messaoudi: conceptualization, data curation, investigation, methodology, writing—original draft, writing—review and editing. Yasmine Fernine: data curation, validation, computations, writing—review and editing. Zehra Seba Keskin: data curation, investigation.

Funding The present study was partly supported by the Sivas Cumhuriyet University Scientific Research Projects Commission.

Data availability There is no dataset provided with this submission.

Declarations

Ethical approval Not applicable.

Competing interests The authors declare no competing interests.

References

1. Rajendran S, Hoang TK, Trudeau ML, Jalil AA, Naushad M, Awual MR (2022) Generation of novel npn (CeO_2-PPy-ZnO) heterojunction for photocatalytic degradation of micro-organic pollutants. Environ Pollut 292:118375
2. Noureen L, Wang Q, Humayun M, Shah WA, Xu Q, Wang X (2022) Recent advances in structural engineering of photocatalysts for environmental remediation. Environ Res 115084.
3. Kubra KT, Salman MS, Znad H, Hasan MN (2021) Efficient encapsulation of toxic dye from wastewater using biodegradable polymeric adsorbent. J Mol Liq 329:115541
4. Naushad M, Alqadami AA, Al-Kahtani AA, Ahamad T, Awual MR, Tatarchuk T (2019) Adsorption of textile dye using para-aminobenzoic acid modified activated carbon: kinetic and equilibrium studies. J Mol Liq 296:112075
5. Yeamin MB, Islam MM, Chowdhury AN, Awual MR (2021) Efficient encapsulation of toxic dyes from wastewater using several biodegradable natural polymers and their composites. J Clean Prod 291:125920
6. Lellis B, Fávaro-Polonio CZ, Pamphile JA, Polonio JC (2019) Effects of textile dyes on health and the environment and bioremediation potential of living organisms. Biotechnol Res Innov 3:275–290. https://doi.org/10.1016/J.BIORI.2019.09.001
7. Jain R, Mathur M, Sikarwar S, Mittal A (2007) Removal of the hazardous dye rhodamine B through photocatalytic and adsorption treatments. J Environ Manage 85(4):956–964
8. Selvam PP, Preethi S, Basakaralingam P, Thinakaran N, Sivasamy A, Sivanesan S (2008) Removal of rhodamine B from aqueous solution by adsorption onto sodium montmorillonite. J Hazard Mater 155(1–2):39–44
9. Selvakumar A, Rangabhashiyam S (2019) Biosorption of rhodamine B onto novel biosorbents from Kappaphycus alvarezii, Gracilaria salicornia and Gracilaria edulis. Environ Pollut 255:113291
10. Priyan VV, Shahnaz T, Suganya E, Sivaprakasam S, Narayanasamy S (2021) Ecotoxicological assessment of micropollutant Diclofenac biosorption on magnetic sawdust: phyto, microbial and fish toxicity studies. J Hazard Mater 403:123532
11. Islam A, Teo SH, Taufiq-Yap YH, Ng CH, Vo DVN, Ibrahim ML, Awual MR (2021) Step towards the sustainable toxic dyes removal and recycling from aqueous solution-a comprehensive review. Resour Conserv Recycl 175:105849
12. Teo SH, Ng CH, Islam A, Abdulkareem-Alsultan G, Joseph CG, Janaun J, Awual R (2021) Sustainabletoxic dyes removal with advanced materials for clean water production: a comprehensive review. J Clean Prod 130039.
13. Kubra KT, Salman MS, Hasan MN (2021) Enhanced toxic dye removal from wastewater using biodegradable polymeric natural adsorbent. J Mol Liq 328:115468
14. Znad H, Abbas K, Hena S, Awual MR (2018) Synthesis a novel multilamellar mesoporous TiO_2/ZSM-5 for photo-catalytic degradation of methyl orange dye in aqueous media. J Environ Chem Eng 6(1):218–227
15. Hasan MM, Shenashen MA, Hasan MN, Znad H, Salman MS, Awual MR (2021) Natural biodegradable polymeric bioadsorbents for efficient cationic dye encapsulation from wastewater. J Mol Liq 323:114587
16. Munjur HM, Hasan MN, Awual MR, Islam MM, Shenashen MA, Iqbal J (2020) Biodegradable natural carbohydrate polymeric sustainable adsorbents for efficient toxic dye removal from wastewater. J Mol Liq 319:114356
17. Paredes-Quevedo LC, González-Caicedo C, Torres-Luna JA, Carriazo JG (2021) Removal of a textile azo-dye (Basic Red 46) in water by efficient adsorption on a natural clay. Water Air Soil Pollut 232(1):1–19
18. Shen T, Wang L, Zhao Q, Guo S, Gao M (2020) Single and simultaneous adsorption of basic dyes by novel organo-vermiculite: a combined experimental and theoretical study. Colloids Surf A Physicochem Eng 601:125059
19. Largo F, Haounati R, Akhouairi S, Ouachtak H, El Haouti R, El Guerdaoui A, Addi AA (2020) Adsorptive removal of both cationic and anionic dyes by using sepiolite clay mineral as adsorbent: experimental and molecular dynamic simulation studies. J Mol Liq 318:114247
20. Shirazi EK, Metzger JW, Fischer K, Hassani AH (2020) Removal of textile dyes from single and binary component systems by Persian bentonite and a mixed adsorbent of bentonite/charred dolomite. Colloids Surf A Physicochem Eng 598:124807
21. Şenol ZM (2021) A chitosan-based composite for adsorption of uranyl ions; mechanism, isothems, kinetics and thermodynamics. Int J Biol Macromol 183:1640–1648
22. Lee SL, Park JH, Kim SH, Kang SW, Cho JS, Jeon JR, Seo DC (2019) Sorption behavior of malachite green onto pristine lignin

to evaluate the possibility as a dye adsorbent by lignin. Appl Biol Chem 62(1):1–10
23. Rosas-Castor JM, Garza-González MT, García-Reyes RB et al (2014) Methylene blue biosorption by pericarp of corn, alfalfa, and agave bagasse wastes. Environ Technol (United Kingdom) 35:1077–1090
24. Abbas M, Trari M (2015) Kinetic, equilibrium and thermodynamic study on the removal of Congo Red from aqueous solutions by adsorption onto apricot stone. Process Saf Environ Prot 98:424–436
25. Zhan Y, Yang L, Lan J et al (2020) (2020) Mussel-inspired polydopamine decorated pomelo peel as a durable biosorbent for adsorption of cationic dyes. Cellul 281(28):453–470
26. Sonu K, Sogani M, Syed Z et al (2020) Enhanced decolorization and treatment of textile dye wastewater through adsorption on acid modified corncob derived biochar. ChemistrySelect 5:12287–12297
27. Dhaouadi F, Sellaoui L, Dotto GL et al (2020) Adsorption of methylene blue on comminuted raw avocado seeds: interpretation of the effect of salts via physical monolayer model. J Mol Liq 305:112815
28. Hou Y, Yan S, Huang G et al (2020) Fabrication of N-doped carbons from waste bamboo shoot shell with high removal efficiency of organic dyes from water. Bioresour Technol 303:122939
29. Kwikima MM, Mateso S, Chebude Y (2021) Potentials of agricultural wastes as the ultimate alternative adsorbent for cadmium removal from wastewater. Rev Sci African 13:e00934
30. Abou-Hadid AF, El-Behairy UA, Elmalih MM et al (2022) Production of efficient carbon fiber from different solid waste residuals for adsorption of hazardous metals from wastewater samples. Biomass Convers Biorefin 1:1–16
31. Tran VA, Vu KB, Vo TTT, Do HH, Bach LG, & Lee SW (2021) Experimental and computational investigation on interaction mechanism of rhodamine B adsorption and photodegradation by zeolite imidazole frameworks-8. Appl Surf Sci 148065.
32. Awual MR (2019) A facile composite material for enhanced cadmium (II) ion capturing from wastewater. J Environ Chem Eng 7(5):103378
33. Awual MR (2019) Mesoporous composite material for efficient lead (II) detection and removal from aqueous media. J Environ Chem Eng 7(3):103124
34. Awual MR, Hasan MM, Rahman MM, Asiri AM (2019) Novel composite material for selective copper (II) detection and removal from aqueous media. J Mol Liq 283:772–780
35. Fernine Y, Salim R, Arrousse N et al (2022) Anti-corrosion performance of Ocimum basilicum seed extract as environmental friendly inhibitors for mild steel in HCl solution: evaluations of electrochemical, EDX, DFT and Monte Carlo. J Mol Liq 355:118867
36. Lu Y, Zhang Y, Zhang K (2022) Renewable biomass resources to access halogen- and phosphorus-free flame retardant thermosets with ultra-low heat release capacity. Chem Eng J 448:137670
37. Hadjiivanov KI, Panayotov DA, Mihaylov MY et al (2021) Power of infrared and Raman spectroscopies to characterize metal-organic frameworks and investigate their interaction with guest molecules. Chem Rev 121:1286–1424
38. Ahmad A, Chowdhary P, Khan N et al (2022) Effect of sewage sludge biochar on the soil nutrient, microbial abundance, and plant biomass: a sustainable approach towards mitigation of solid waste. Chemosphere 287:132112
39. Arrousse N, Fernine Y, Al-Zaqri N et al (2022) Thiophene derivatives as corrosion inhibitors for 2024–T3 aluminum alloy in hydrochloric acid medium. RSC Adv 12:10321–10335
40. Nizam NUM, Hanafiah MM, Mahmoudi E et al (2021) (2021) The removal of anionic and cationic dyes from an aqueous solution using biomass-based activated carbon. Sci Reports 111(11):1–17
41 Yang J, Shojaei S, Shojaei S (2022) Removal of drug and dye from aqueous solutions by graphene oxide: adsorption studies and chemometrics methods. npj Clean Water 5:1–10
42. El Khomri M, El Messaoudi N, Dbik A et al (2021) Regeneration of argan nutshell and almond shell using HNO_3 for their reusability to remove cationic dye from aqueous solution. Chem Eng Commun 209:1304–1315
43. El Messaoudi N, El Khomri M, Chegini ZG et al (2022) Dye removal from aqueous solution using nanocomposite synthesized from oxalic acid-modified agricultural solid waste and $ZnFe_2O_4$ nanoparticles. Nanotechnol Environ Eng 7:797–811
44. Elgarahy AM, Elwakeel KZ, Mohammad SH, Elshoubaky GA (2021) A critical review of biosorption of dyes, heavy metals and metalloids from wastewater as an efficient and green process. Clean Eng Technol 4:100209
45. Gul S, Gul H, Gul M et al (2022) Enhanced adsorption of rhodamine B on biomass of cypress/false cypress (Chamaecyparis lawsoniana) fruit: optimization and kinetic study. Water 14:2987
46. Awual MR (2015) A novel facial composite adsorbent for enhanced copper (II) detection and removal from wastewater. Chem Eng J 266:368–375
47. Hasan MN, Shenashen MA, Hasan MM, Znad H, Awual MR (2021) Assessing of cesium removal from wastewater using functionalized wood cellulosic adsorbent. Chemosphere 270:128668
48. Khandaker S, Chowdhury MF, Awual MR, Islam A, Kuba T (2021) Efficient cesium encapsulation from contaminated water by cellulosic biomass based activated wood charcoal. Chemosphere 262:127801
49. Şenol ZM (2022) Effective biosorption of Allura red dye from aqueous solutions by the dried-lichen (Pseudoevernia furfuracea) biomass. J Environ Anal Chem 102(16):4550–4564
50. Sevim F, Lacin O, Ediz EF, Demir F (2021) Adsorption capacity, isotherm, kinetic, and thermodynamic studies on adsorption behavior of malachite green onto natural red clay. Environ Prog Sustain Energy 40:13471
51. Shen K, Gondal MA (2017) Removal of hazardous rhodamine dye from water by adsorption onto exhausted coffee ground. J Saudi Chem Soc 21:120-S127
52. Singh S, Parveen N, Gupta H (2018) Adsorptive decontamination of rhodamine-B from water using banana peel powder: a biosorbent. Environ Technol Innov 12:189–195
53. Shah J, Rasul Jan M, Haq A (2013) Khan Y (2013) Removal of rhodamine B from aqueous solutions and wastewater by walnut shells: kinetics, equilibrium and thermodynamics studies. Front Chem Sci Eng 74(7):428–436
54. Gupta VK, Jain R, Siddiqui MN et al (2010) Equilibrium and thermodynamic studies on the adsorption of the dye rhodamine-B onto mustard cake and activated carbon. J Chem Eng Data 55:5225–5229
55. Kerkez Ö (2014) Bayazit ŞS (2014) Magnetite decorated multi-walled carbon nanotubes for removal of toxic dyes from aqueous solutions. J Nanoparticle Res 166(16):1–11
56. Kumar S, Bhanjana G, Jangra K et al (2014) Utilization of carbon nanotubes for the removal of rhodamine B dye from aqueous solutions. J Nanosci Nanotechnol 14:4331–4336
57. Chen M, Shang T, Fang W, Diao G (2011) Study on adsorption and desorption properties of the starch grafted p-tert-butylcalix[n]arene for butyl rhodamine B solution. J Hazard Mater 185:914–921
58. Koyuncu M, Kul AR (2014) Thermodynamics and adsorption studies of dye (rhodamine-b) onto natural diatomite. Physicochem Probl Miner Process 50:631–643
59. Simonin JP (2016) On the comparison of pseudo-first order and pseudo-second order rate laws in the modeling of adsorption kinetics. Chem Eng J 300:254–263

60. Largitte L, Pasquier R (2016) A review of the kinetics adsorption models and their application to the adsorption of lead by an activated carbon. Chem Eng Res Des 109:495–504
61. Awual MR, Hasan MM, Islam A, Asiri AM, Rahman MM (2020) Optimization of an innovative composited material for effective monitoring and removal of cobalt (II) from wastewater. J Mol Liq 298:112035
62. Lima EC, Hosseini-Bandegharaei A, Moreno-Piraján JC, Anastopoulos I (2019) A critical review of the estimation of the thermodynamic parameters on adsorption equilibria. Wrong use of equilibrium constant in the Van't Hoof equation for calculation of thermodynamic parameters of adsorption. J Mol Liq 273:425–434
63. Kubra KT, Salman MS, Hasan MN, Islam A, Teo SH, Hasan MM, Awual MR (2021) Sustainable detection and capturing of cerium (III) using ligand embedded solid-state conjugate adsorbent. J Mol Liq 338:116667
64. Awual MR, Hasan MM, Znad H (2015) Organic–inorganic based nano-conjugate adsorbent for selective palladium (II) detection, separation and recovery. Chem Eng J 259:611–619
65. Fernine Y, Arrousse N, Haldhar R et al (2022) Synthesis and characterization of phenolphthalein derivatives, detailed theoretical DFT computation/molecular simulation, and prevention of AA2024-T3 corrosion in medium 3.5% NaCl. J Taiwan Inst Chem Eng 140:104556